TABLE OF CONTENTS

MATERIAL AND METHODS

Synthesis: Commercially available reagents and solvents were used without further purification other than those detailed below. THF was distilled from sodium/benzophenone prior to use. Light petroleum refers to the fraction with bp 40-60°C. Reactions were stirred magnetically, unless otherwise indicated. Analytical thin layer chromatography was carried out using aluminum backed plates coated with Merck Kieselgel 60 GF254 and visualized under UV light (at 254 and 360 nm). Chromatography was carried out using Teledyne Isco CombiFlash® Rf 400 (UV detection 200-360nm), over standard silica cartridges (Redisep® Isco standard (40 - 60µ) or Gold (20 - 40µ)). ^{1}H and ^{13}C NMR spectra were recorded using Bruker 300 MHz instruments (^{1}H frequency, corresponding ^{13}C frequency: 75 MHz); chemical shifts were recorded in ppm and J values in Hz. In the ^{13}C NMR spectra, signals corresponding to CH, CH$_2$ or Me groups, assigned from DEPT, are noted; all others are C. The residual signal for the CD$_2$Cl$_2$ is 5.32 ppm for the proton and 54.00 ppm for the carbon. The following abbreviations have been used for the NMR assignment: s for singlet, d for doublet, t for triplet and m for multiplet. High resolution mass spectra were recorded at the Centre Régional de Mesures Physiques de l'Ouest (Rennes) on (i) Bruker MicrO-Tof-Q II (Source: Atmospheric Pressure Chemical Ionisation (APCI - direct introduction (ASAP–Atmospheric Solids Analysis Probe) at a temperature of 30°C - positive mode) or on (ii) Waters Q-Tof II (source: electrospray (ESI)).

X Ray: ($C_{31}H_{21}NO_2S$); *M* = 471.56. APEXII, Bruker-AXS diffractometer, Mo-Kα radiation (λ = 0.71073 Å), *T* = 150(2) K; triclinic *P-1* (I.T.#2), a = 8.8667(3), b = 11.8588(3), c = 15.4264(4) Å, α = 112.2520(10), β = 95.2040(10), γ = 94.2860(10) °, *V* = 1484.57(7) Å^3. *Z* = 2, *d* = 1.055 g.cm^{-3}, μ = 0.133 mm^{-1}. The structure was solved by direct methods using the SIR97 program[1], and then refined with full-matrix least-square methods based on F2 (SHELXL-97)[2] with the aid of the WINGX[3] program. All non-hydrogen atoms were refined with anisotropic atomic displacement parameters. H atoms were finally included in their calculated positions. A final refinement on F2 with 7286 unique intensities and 424 parameters converged at ωR(F2) = 0.1606 (R(F) = 0.058) for 6014 observed reflections with I > 2σ(I).

Spectroscopic studies: Cyclohexane (AnalaR NORMAPUR, VWR), Toluene (Spectrometric grade 99,7%, Alfa Aesar), Chloroform (AnalaR, NORMAPUR, VWR), Ethyl Acetate (for analysis, Carlo Erba), Acetonitrile (Anhydrous for analysis, Carlo Erba), 2-Methylpentane (99+%, Alfa Aesar), Methylcyclohexane (>99.0%, TCI), H_2SO_4 1N solution in water (Standard solution, Alfa Aesar), and Quinine sulfate dihydrate (99+%, Alfa Aesar) were used without further purification. UV-visible spectra were recorded using a UV-Visible spectrophotometer SHIMADZU UV-1605. The optical gap was calculated from the absorption edge of the UV-vis absorption spectrum using the formula ΔE^{opt} (eV) = hc/λ, λ being the absorption edge (in meter). With h = 6.63×10^{-34} J.s (1eV = 1.6×10^{-19} J) and c = 3.0×10^{8} m.s^{-1}, this equation may be simplified as: ΔE^{opt} (eV) = 1237.5/ λ (in nm). Photoluminescence spectra were recorded with a PTI spectrofluorimeter (PTI-814 PDS, MD 5020, LPS 220B) using a xenon lamp. Quantum yields in solution (ϕ_{sol}) were calculated relative to quinine sulfate (ϕ_{sol} = 0.546 in H_2SO_4 1N). ϕ_{sol} was determined according to the following equation (1),

$$\phi_{sol}=\phi_{ref}\times100\times\frac{(Ts\times Ar)}{(Tr\times As)}\left(\frac{n_s}{n_r}\right)^2 \quad (1)$$

where, subscripts s and r refer respectively to the sample and reference. The integrated area of the emission peak in arbitrary units is given as T, n is the refracting index of the solvent (n_s = 1.427 for Cyclohexane) and A is the absorbance. 4 solutions of different concentration of the substrate (A<0.1) were prepared and 4 solutions of quinine sulfate, and absorption and emission spectrum were recorded (excitation at 336 nm for the quinine sulfate). Slope of the integrated emission intensity vs absorbance gave Tx/Ax. 4 quantum yields are then calculated and the average value is reported. IR spectra were recorded on a Bruker Vertex 70 using a diamond crystal MIRacle ATR (Pike).

Low temperature (77K) measurements were performed in methylcyclohexane / 2-methylpentane 1/1 solution which freezes as a transparent glassy matrix. Measurements were carried using a single-block quartz cuvette containing the solution, which was placed in an Oxford Optistat cryostat cooled with liquid nitrogen, equipped itself with three quartz optical windows. Phosphorescence emission spectra were recorded on a Horiba Jobin-Yvon Fluorolog FL3-221 in the continuous excitation mode.

Electrochemical studies: All electrochemical experiments were performed under an argon atmosphere, using a Pt disk electrode (diameter 1 mm), the counter electrode was a vitreous carbon rod and the reference electrode was a silver wire in a 0.1 M $AgNO_3$ solution in CH_3CN. Ferrocene was added to the electrolyte solution at the end of a series of experiments. The ferrocene/ferrocenium (Fc/Fc^+) couple served as internal standard. The three electrode cell was connected to a PAR Model 273 potentiostat/galvanostat (PAR, EG&G, USA) monitored with the ECHEM Software. Activated Al_2O_3 was added in the electrolytic solution to remove excess moisture. For a further comparison of the electrochemical and optical properties, all potentials are referred to the SCE electrode that was calibrated at 0.405 V vs. Fc/Fc^+ system. Following the work of Jenekhe,[4] we estimated the electron affinity (EA) or lowest unoccupied molecular orbital (LUMO) and the ionization potential (IP) or highest occupied molecular orbital (HOMO) from the redox data. The LUMO level was calculated from: LUMO (eV)= -[E_{onset}^{red} (vs SCE) + 4.4] and the HOMO level from: HOMO (eV) = -[E_{onset}^{ox} (vs SCE) + 4.4], based on an SCE energy level of 4.4 eV relative to the vacuum. The electrochemical gap was calculated from : ΔE^{el} =|HOMO-LUMO| (in eV).[4,5]

Theoretical modeling : Full geometry optimization with Density functional theory (DFT)[6,7] and Time-Dependent Density Functional Theory (TD-DFT) calculations were performed with the hybrid Becke-3 parameter exchange[8-10] functional and the Lee-Yang-Parr non-local correlation functional[11] (B3LYP) implemented in the Gaussian 09 (Revision B.01) program suite[12] using the 6-311G+(d,p) basis set and the default convergence criterion implemented in the program. The figures were generated with GaussView 5.0. The computed triplet adiabatic S^0 to T^1 excitation energies were calculated from the difference between the total energy of the molecule in their respective optimized singlet and triplet states. Calculations were carried out at the CINES, "Centre Informatique National de l'Enseignement Supérieur" in Montpellier.

Device fabrication and characterization:

OLEDs based on a multilayer structure have been fabricated onto patterned ITO coated glass substrates from XinYan Tech (thickness: 100 nm and sheet resistance: less of 20 W/m). The organic materials (from Aldrich and Lumtec) are deposited onto the ITO anode by sublimation under high vacuum ($< 10^{-6}$ Torr) at a rate of 0.2 – 0.3 nm/s. The structure of the device is the following: ITO/CuPc (10 nm)/NPB (40 nm)/TCTA (10 nm)/ **EML** (20 nm)/TPBi (40 nm)/LiF (1.2 nm)/Al (100 nm). In this device, ITO is used as the anode, CuPc (copper phtalocyanine) is the hole injecting layer, NPB (N,N'-di(1-naphtyl)-N,N'-diphenyl-[1,1'-biphenyl]-4,4'-diamine) is the hole-transporting layer, TCTA (4,4',4''-Tris(carbazol-9-yl)-triphenylamine) is the electron blocking layer, TPBI (1,3,5-Tris(1-phenyl-1H-benzimidazol-2-yl)benzene) is both the electron transporting layer and the hole blocking layer and a thin film of lithium fluoride covered with aluminum is the cathode. The entire device is fabricated in the same run without breaking the vacuum. In this study, the thicknesses of the different organic layers were kept constant for all the devices. The active area of the devices defined by the overlap of the ITO anode and the metallic cathode was 0.3 cm². Emissive layer (EML) was composed of either **SPA-TXO$_2$** doped with Tris[2-phenylpyridinato-C2,N]iridium(III) or Bis[2-(4,6-difluorophenyl)pyridinato-C2,N](picolinato)iridium(III).

The current-voltage-luminance (I-V-L) characteristics of the devices were measured with a regulated power supply (Laboratory Power Supply EA-PS 3032-10B) combined with a multimeter and a 1 cm² area silicon calibrated photodiode (Hamamatsu). The spectral emission was recorded with a SpectraScan PR650 spectrophotometer. All the measurements were performed at room temperature and at ambient atmosphere with no further encapsulation of devices.

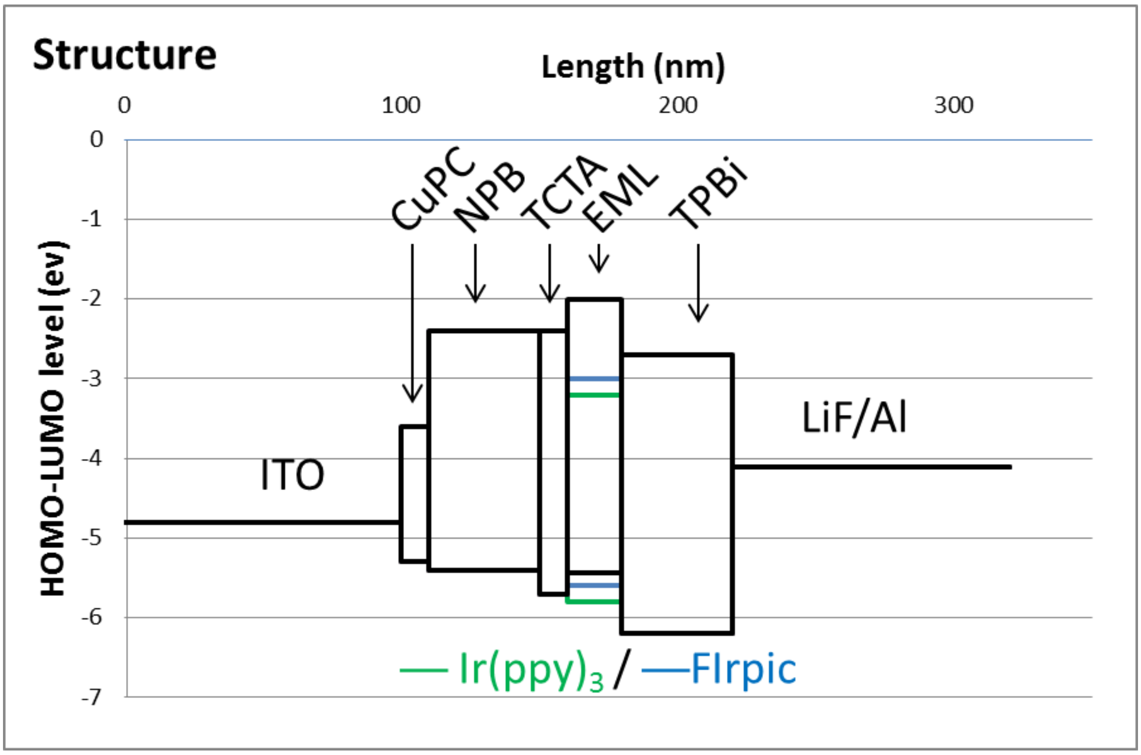

S1. Structure of devices

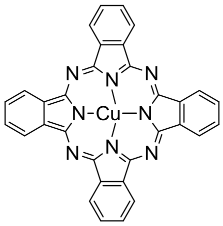

copper phthalocianine (CuPc)

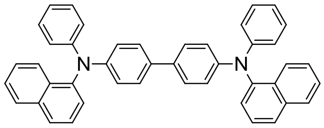

N,N'-Di-[(1-naphthyl)-N,N'-diphenyl]-1,1'-biphenyl)-4,4'-diamine (NPB)

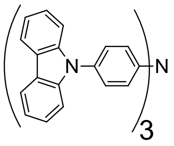

Tris(4-carbazoyl-9-ylphenyl) amine (TCTA)

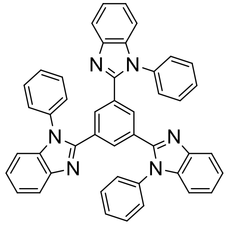

1,3,5-tris(N-phenylbenzimidazol-2-yl) benzene (TPBI)

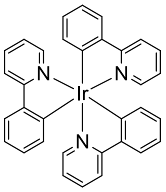

Tris[2-phenylpyridinato-C^2,N]iridium(III) ($IrPPy_3$)

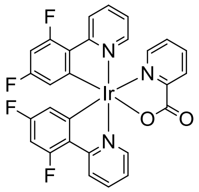

Bis[2-(4,6-difluorophenyl)pyridinato-C^2,N](picolinato)iridium(III) (FIrpic)

S2. Organic component of devices

Synthesis

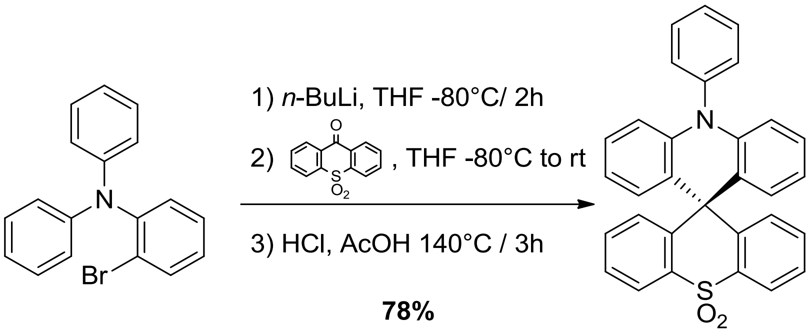

SPA-TXO$_2$

10-phenyl-10H-spiro[acridine-9,9'-thioxanthene] 10',10'-dioxide (SPA-TXO$_2$)

2-bromo-N,N-diphénylaniline (1.04 g, 3.2 mmol, 1.1 eq) was dissolved in dry THF (20 mL) and cooled down to -78°C. A 2.5 M pentane solution of *n*-BuLi (1.3 mL, 3.2 mmol, 1.1 eq) was added dropwise into the solution at -78°C. The resulting mixture was stirred at the same temperature for 2h and 9*H*-thioxanthen-9-one 10,10-dioxide[13] (0.73 g, 3.0 mmol, 1 eq) dissolved in dry THF (50 mL) was then added dropwise, and temperature was allowed to raise to 20°C overnight. Water (50 mL) was added, and the mixture was extracted with dichloromethane (3 x 50 mL). The combined organic extracts were dried over anhydrous magnesium sulfate, filtered, and concentrated under reduced pressure. The residue was then dissolved in 50 mL of glacial acetic acid and heated to reflux. 5 mL of 37% HCl solution was then added and the reaction mixture was kept refluxing 3h. Solvents were then removed under reduced pressure and the residue was purified by flash chromatography on silica gel (petroleum/ethyl acetate, see below) to give a colorless solid (1.3 g, 2.3 mmol). Yield: 78 %.
mp (Toluene) = 308-310°C;[column conditions: Silica cartridge 12 g (Serlabo); solid deposit on Celite®; $\lambda_{detection}$: (254 nm, 280 nm) ; at 30 mL/min; 0-20 min: ethyl acetate/light petroleum 1/9, 20-40 min ethyl acetate/light petroleum 6/4); collected fraction: 24-35 min].^{1}H NMR (300 MHz, CD_2Cl_2) δ 8.12 (ddd, *J* = 3.9, 2.4, 0.4 Hz, 2H, Ha), 7.75 (t, *J* = 7.5 Hz, 2H, Hb), 7.62 (tt, *J* = 7.5, 1.3 Hz, 1H, Hc), 7.53 – 7.45 (m, 6H, Hd), 7.45 – 7.40 (m, 2H, He), 6.91 (ddd, *J* = 8.4, 7.1, 1.6 Hz, 2H, Hf), 6.75 (dd, *J* = 7.9, 1.6 Hz, 2H, Hg), 6.63 (ddd, *J* = 7.9, 7.1, 1.0 Hz, 2H, Hh), 6.34 (dd, *J* = 8.4, 1.0 Hz, 2H, Hi).^{13}C NMR (75 MHz, CD_2Cl_2) δ 146.93 (C,I), 140.88 (C,II), 139.51 (C,III), 134.35 (C,IV), 133.98 (CH,V), 133.26 (CH,VI), 132.24 (CH,VII), 131.74 (CH,VIII), 131.44 (CH,IX), 129.22 (CH,X), 128.18 (CH,XI), 128.08 (CH,XII), 127.56 (C,XIII), 122.28 (CH,XIV), 121.51 (Ch,XV), 115.55 (CH,XVI), 48.90 (spiroC,XVII). HRMS (ASAP): (Found: $[M+H]^+$, 472.1369; $C_{31}H_{22}NO_2S$ required 472.13713). Elemental analysis calculated (%) for $C_{31}H_{21}NO_2S$: C 78.96, H 4.49, N 2.97, O 6.79, S 6.80 found: C 78.95, H 4.74, N 3.17, O 6.79, S 6.80.

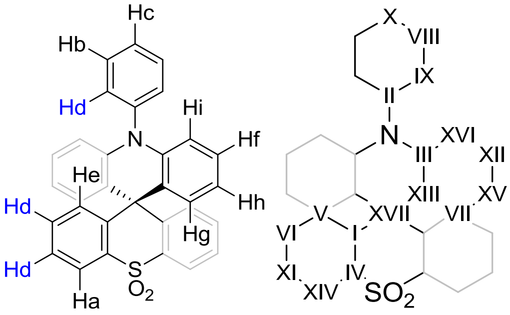

Structural properties

Single crystals of **SPA-TXO$_2$** were obtained by vapor diffusion of pentane in a CDCl$_3$ solution.

Table 1.Crystal data and structure refinement for **SPA-TXO$_2$**.

Identification code	squeezed	
Empirical formula	C31 H21 N O2 S	
Formula weight	471.56	
Temperature	150(2) K	
Wavelength	0.71073 Å	
Crystal system	Triclinic	
Space group	P-1	
Unit cell dimensions	a = 8.8667(3) Å	α = 112.2520(10)°.
	b = 11.8588(3) Å	β = 95.2040(10)°.
	c = 15.4264(4) Å	γ = 94.2860(10)°.
Volume	1484.57(7) Å^3	
Z	2	
Density (calculated)	1.055 Mg/m^3	
Absorption coefficient	0.133 mm^{-1}	
F(000)	492	
Crystal size	0.45 x 0.32 x 0.21 mm^3	
Theta range for data collection	1.44 to 27.55°.	
Index ranges	-11<=h<=11, -10<=k<=15, -20<=l<=18	
Reflections collected	13134	
Independent reflections	6766 [R(int) = 0.0248]	
Completeness to theta = 27.55°	98.6 %	
Absorption correction	Semi-empirical from equivalents	
Max. and min. transmission	0.972 and 0.950	
Refinement method	Full-matrix least-squares on F^2	
Data / restraints / parameters	6766 / 0 / 317	
Goodness-of-fit on F^2	1.111	
Final R indices [I>2sigma(I)]	R1 = 0.0667, wR2 = 0.1868	
R indices (all data)	R1 = 0.0792, wR2 = 0.1940	
Largest diff. peak and hole	0.601 and -0.421 e.Å^{-3}	

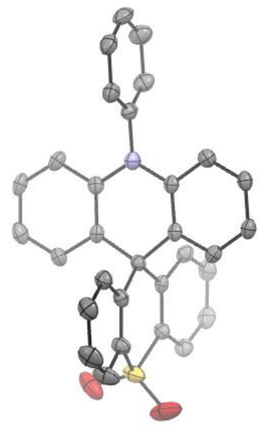

Table 2. Thioxanthene-dioxide characteristics

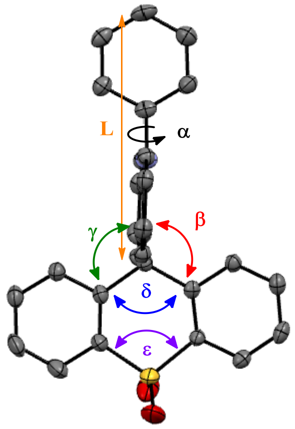	Molecule radius (L)	7.14 Å
	Phenyl/acridine twist angle (**α**)	88°
	TXO_2 angle 1 (**β**)	119°
	TXO_2 angle 2 (γ)	125°
	TXO_2 angle 3 (δ)	115°
	TXO_2 C-S-C angle (ε)	104°

Table 3. Phenyl-acridine characteristics

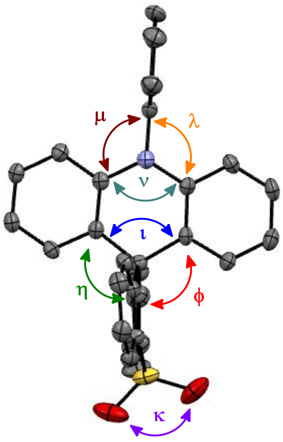	C-N-Ph angle 1 (λ)	119°
	C-N-Ph angle 2 (μ)	119°
	C-N-C angle 3 (ν)	121°
	Acridine angle 1 (ι)	111°
	Acridine angle 2 (ϕ)	121°
	Acridine angle 3 (η)	128°
	TXO_2 O-S-O angle (κ)	117°

Table 4. Fragments torsion

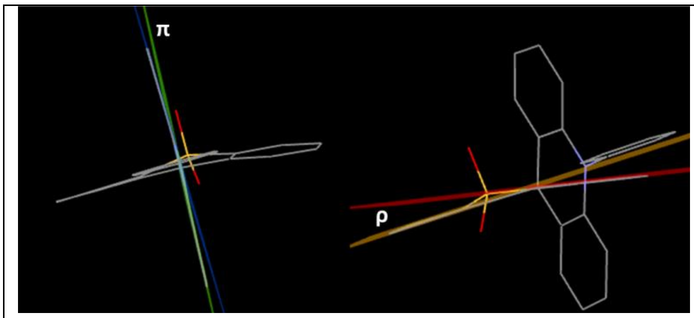	Acridine benzene-rings angle (π)	3.3°
	TXO_2 benzene-rings angle (ρ)	11.5°

Thermal properties

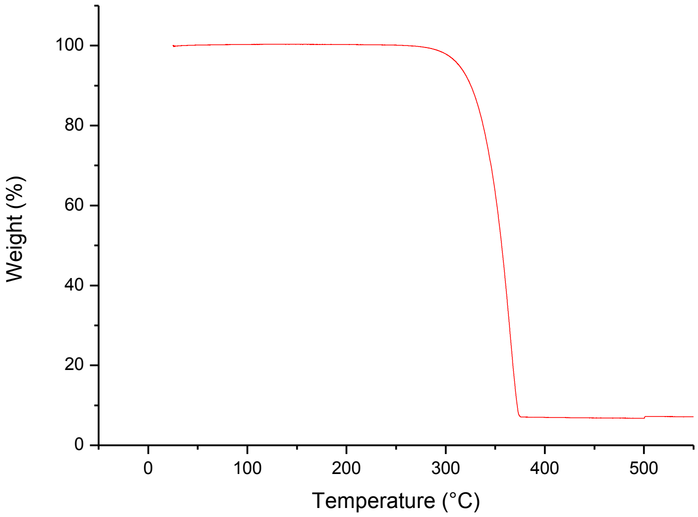

S3. TGA analysis of **SPA-TXO$_2$**, under N_2 at 10°C.min^{-1}

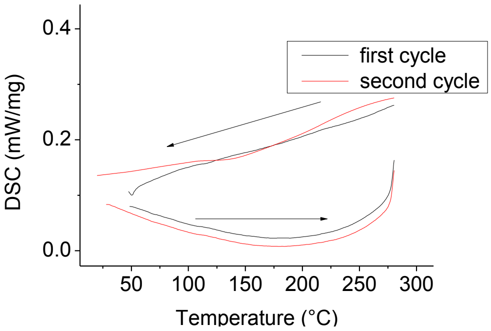

S4. DSC analysis of **SPA-TXO$_2$**, under N_2 at 10°C.min^{-1}

Photophysical properties

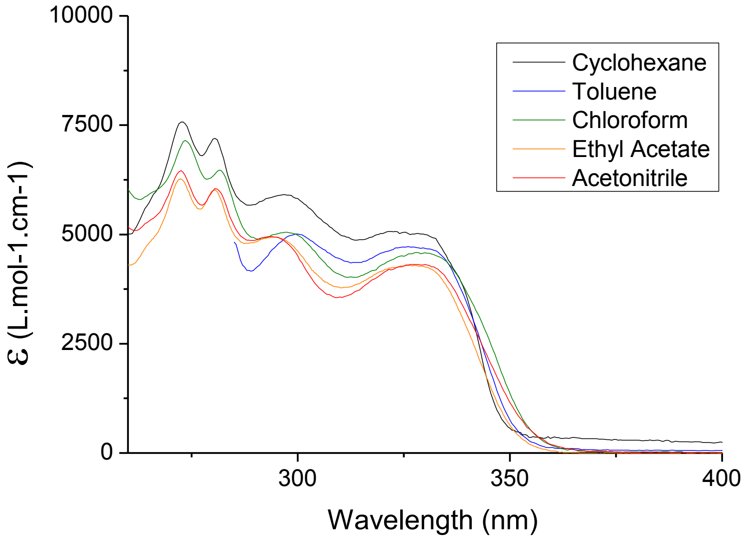

S5. UV-Vis absorption spectra of solutions of **SPA-TXO$_2$** in different solvents

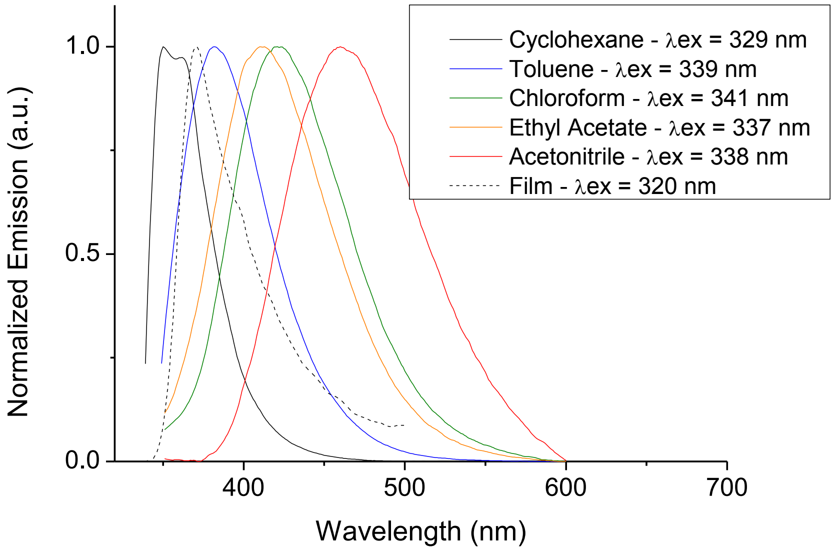

S6. Emission spectra of **SPA-TXO$_2$** in solution and as a spin-coated film, normalized at λmax

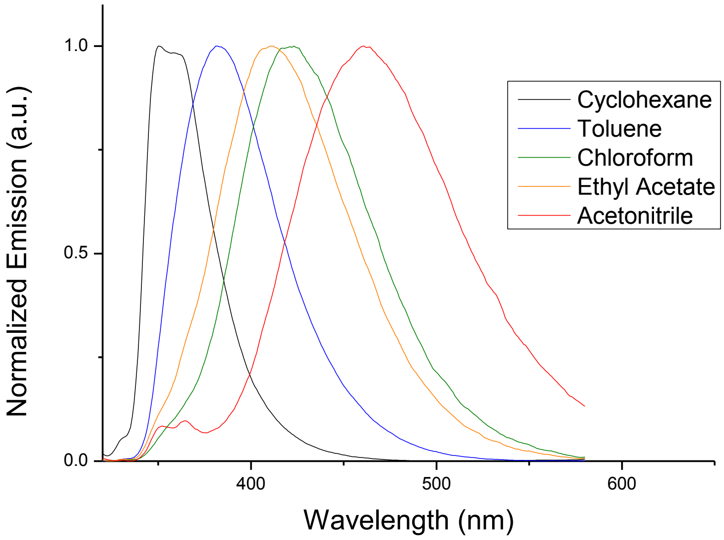

S7. Emssion spectra of **SPA-TXO$_2$** in different solvents with λ_{EX} = 300 nm, normalized at λmax

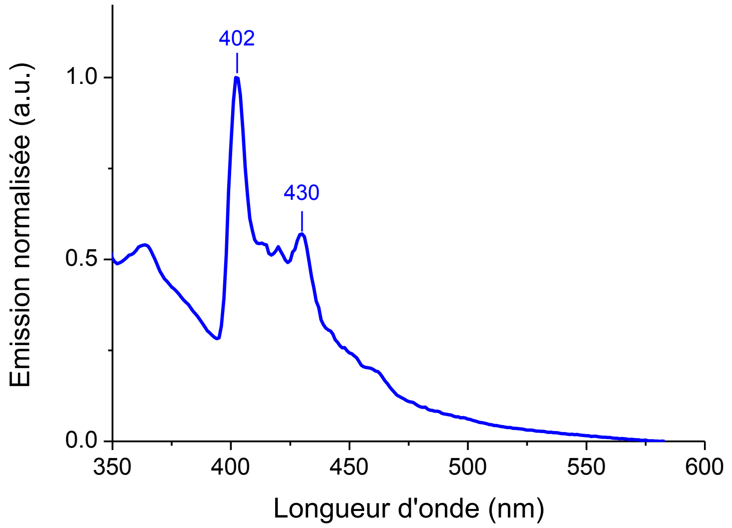

S8. Emission spectra at 77K of **SPA-TXO$_2$** in methylcyclohexane/2-methylpentane, λex = 300 nm, E_T was calculated with the highest energy phosphorescence transition : 402 nm (3.08 eV), normalized on the highest energy phosphorescence transition.

Electrochemical properties

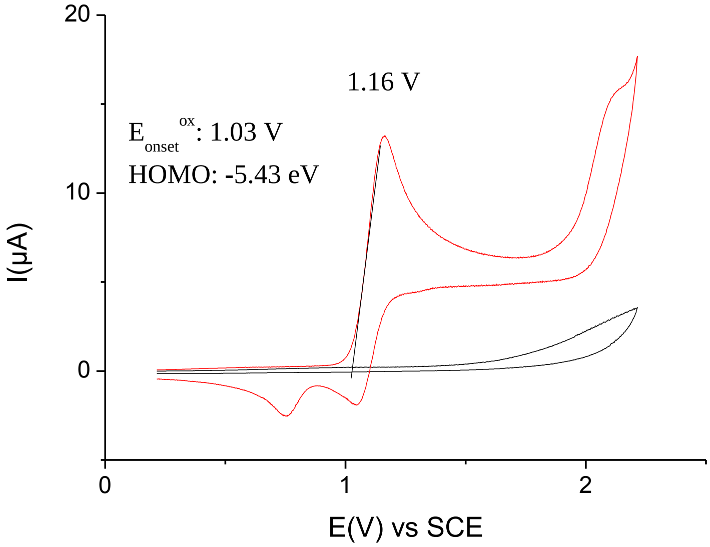

S9. Oxidation CV of a solution of CH_2Cl_2 + 0.2 M Bu_4NPF_6 (black) and after addition of **SPA-TXO$_2$** ($3\ 10^{-3}$ mol.L^{-1}) (red). Working electrode: platinum disk diameter 1 mm, sweep-rate 100 mV/s.

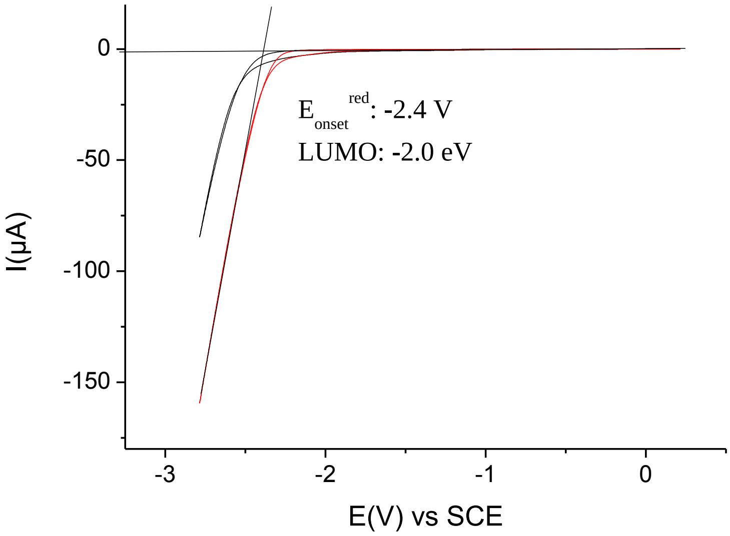

S10. Reduction CV of a solution of CH_2Cl_2 + 0.2 M Bu_4NPF_6 (black) and after addition of **SPA-TXO$_2$** ($3\ 10^{-3}$ mol.L^{-1}) (red). Working electrode: platinum disk diameter 1 mm, sweep-rate 100 mV/s.

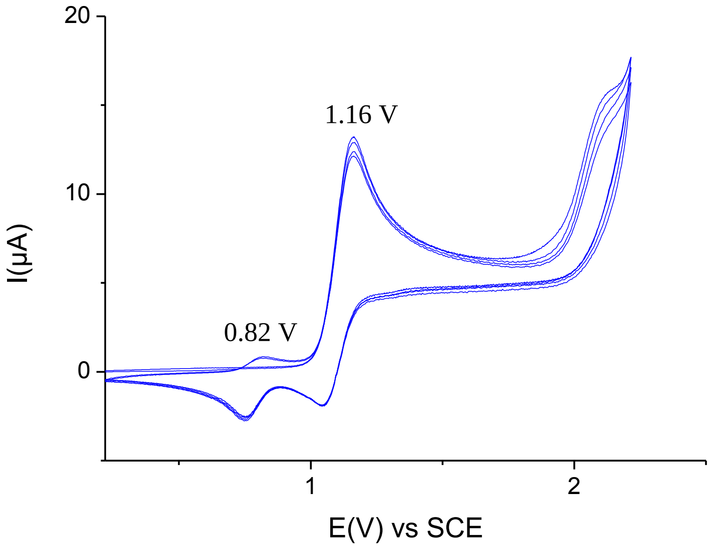

S11. 4 successive oxidation CV between in the [0.2 V – 2.2] range, of a solution of of **SPA-TXO$_2$** (3 10^{-3} mol.L^{-1}) in CH_2Cl_2 + 0.2 M Bu_4NPF_6. Working electrode: platinum disk diameter 1 mm, sweep-rate 100 mV/s.

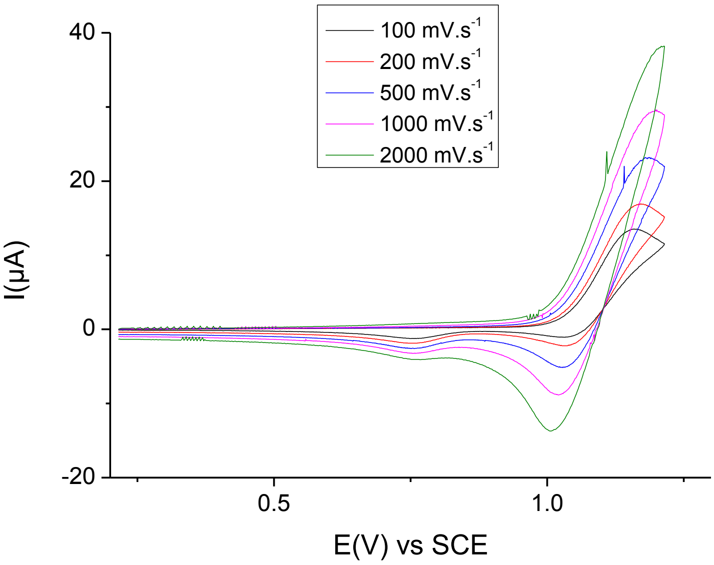

S12. Oxidation CV of a solution of CH_2Cl_2 + 0.2 M Bu_4NPF_6 (black) and after addition of **SPA-TXO$_2$** (3 10^{-3} mol.L^{-1}) (red). Working electrode: platinum disk diameter 1 mm, with increasing sweep-rate, partial reversibility is observed at high sweep-rate

Theoretical modeling

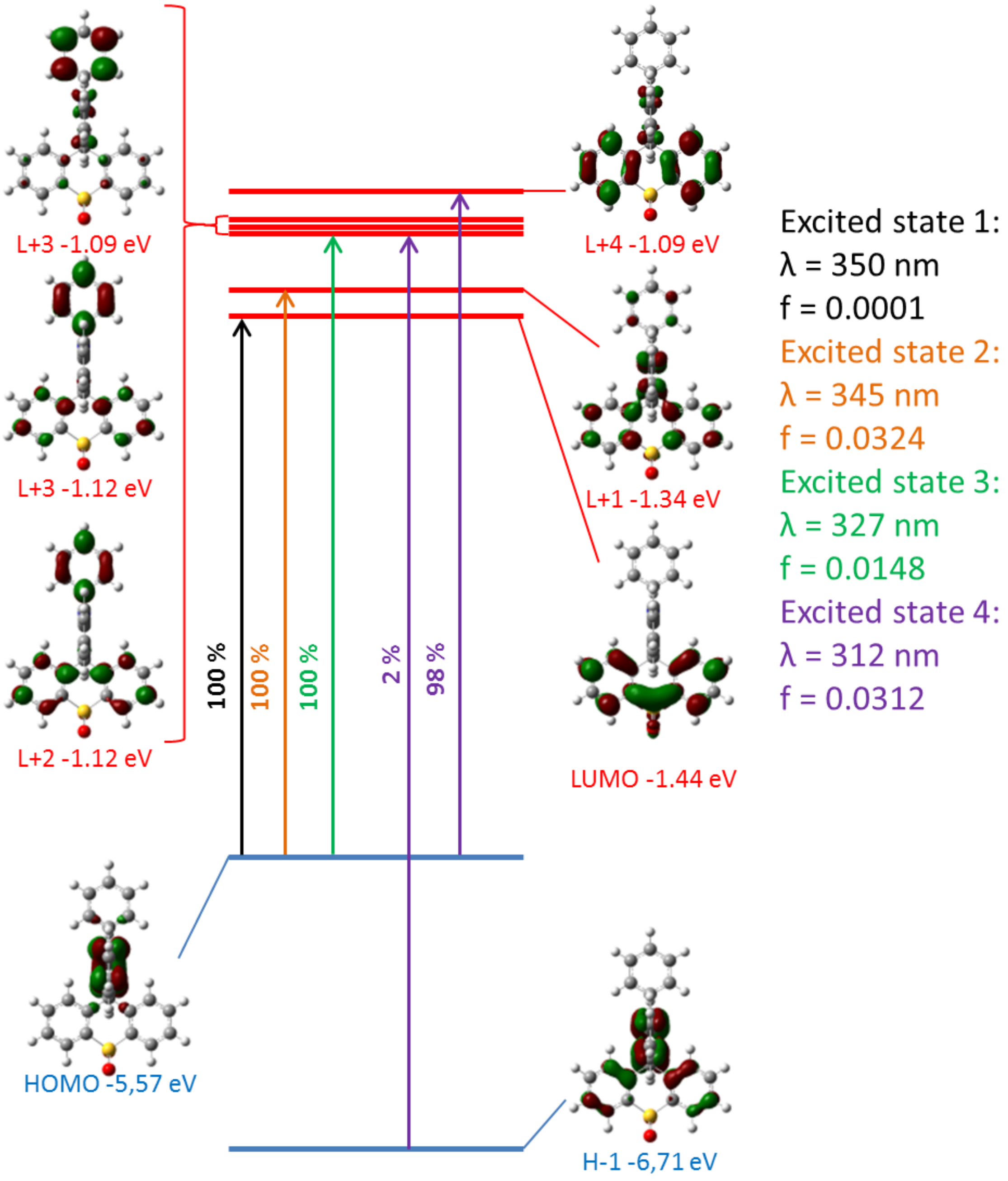

S13. Calculated frontier molecular orbitals by DFT and the 4th first calculated electronic transitions by TD-DFT of **SPA-TXO$_2$**, after geometry optimization with DFT B3LYP/6-311+G(d,p), shown with a cut-off 0.04 [e bohr^{-3}]$^{1/2}$.

Summary

Table 5.Summary of solvatochromic properties

	Δf [a]	λ_{ABS} (nm)	λ_{EM} (nm)	Φ_{PL} (%) (λ_{EX})	$\Delta\nu$ [b] (cm^{-1})	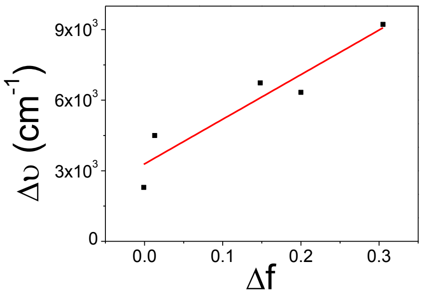 y = $1{,}90.10^4$ x + $3{,}39.10^3$
Cyclohexane	-0.001	323	351	4.1 (323)	2293	
Toluene	0.013	326	382	2.3 (326)	4497	
Chloroform	0.148	328	421	1.2 (328)	6735	
Ethyl Acetate	0.200	326	410	1.7 (326)	6332	
Acetonitrile	0.305	323	461	1.4 (323)	8564	

Radius [c] (Å)	8,3
μ [d] / Δμ [e] / μ* [f] (D)	7,5 / 32,6 / 40,1

a. orientation polarizability calculated from dielectric constant (ε)[14] and index of refraction (n)[14]: $\Delta f = (\varepsilon-1)/(2\varepsilon-1)-(n^2-1)/(2n^2-1)$ **b.** Stokes shift **c.** from RX datas **d.** ground state dipole moment from DFT optimisation at 6-311+G(d,p) level of theory without solvatation **e.** from Lippert-Mataga equation, radius "r", Planck constant "h", celerity "c" and slope of curve Δv vs Δf: $(\Delta\mu)^2 = r^3.h.c.slope/2$, **f.** excited state dipole moment $\mu^* = \mu+\Delta\mu$.

Table 6. Summary of other properties

			SPA-TXO_2
λ_{ABS} (ε) [a]		[nm] ([10^3.L.mol^{-1}.cm^{-1}])	323 (5.1), 297 (5.9), 281 (7.2), 273 (7.6)
λ_{EM} (λ_{ex}) [a]		[nm]	351(329)
λ_{EM} (λ_{ex}) [b]		[nm]	363 (300)
Φ_{PL}(λ_{ex}) [a]		/	4.1 (323)
Eox_{onset} [d]		[V]	1.03
$Ered_{onset}$ [d]		[V]	-2.4
HOMO	El[e]/Calc[f]	[eV]	-5.43 / -5.57
LUMO	El[e]/Calc[f]	[eV]	-2.00 / -1.44
ΔE	Opt[a,f]/El[e]/Calc[g]	[eV]	3.56 / 3.43 / 4.13
E_T	Opt[e]/Calc[d]	[eV]	3.08 / 3.18
S-T	Opt[c,g]/Calc[d]	[eV]	0.49 / 0.95
Td[h]		[°C]	313

a. in cyclohexane, **b.** in thin film **c.** in mehtylcyclohexane:2-methylpentane 1:1 **d.** oxidation and reduciton onset potential measured in CH_2Cl_2 with 0.2 M Bu_4NPF_6. Working electrode: platinum disk diameter 1 mm, sweep-rate 100 mV/s **e.** from redox onset potentials, **f.** determined with the edge of the UV-Vis absorption spectrum using E(eV) = 1237.5/λ(nm) **f.** at 6-311+G(d,p) level of theory without solvatation, **g.** Calculated with the first phosphorescent transition at 77k, using E_T(eV) = 1237.5/λ_{PHOS}. **h.** TGA analysis was performed under N_2.

SPA-TXO_2 Devices

Table 7. Properties of SPA-TXO_2 devices

Sample	Vs[a] [V]	EQE[b] [%]	Current Efficiency[b] [cd/A]	Power Efficiency[b] [lm/W]	CIE (x;y) at 10 mA/cm²
undoped	4.2	0.5 / 0.6 / Ø	0.60 / 0.75 / Ø	0.30 / 0.35 / Ø	0.24; 0.29
FIrpic 9%	3.2	9.0 / 8.7 / 9.4	22.2 / 21.4 / 23.1	11.4 / 16.1 / 13.8	0.17; 0.40
FIrpic 15%	3.1	10.9 / 11.9 / 11.6	26.3 / 28.6 / 28.1	14.0 / 22.0 / 16.9	0.17; 0.41
FIrpic 21%	3.1	10.1 / 6.1 / 11.3	25.2 / 15.1 / 28.2	13.2 / 11.3 / 17.0	0.17; 0.42
FIrpic 26%	3.2	11.4 / 12.0 / 12.0	28.6 / 30.0 / 30.2	14.6 / 22.0 / 17.8	0.17; 0.42
$Ir(ppy)_3$ 9%	3.1	14.8 / 15.2 / 16.3	54.9 / 56.2 / 60.4	26.8 / 43.1 / 36.1	0.30; 0.63
$Ir(ppy)_3$ 19%	3.1	11.9 / 13.2 / 12.7	42.3 / 46.8 / 45.0	21.2 / 34.2 / 26.5	0.31; 0.63

a\ at 1 cd.m^{-2}, **b**\ at 10 mA.cm^{-2} / at 100 cd.m^{-2} / at 1000 cd.m^{-2}..

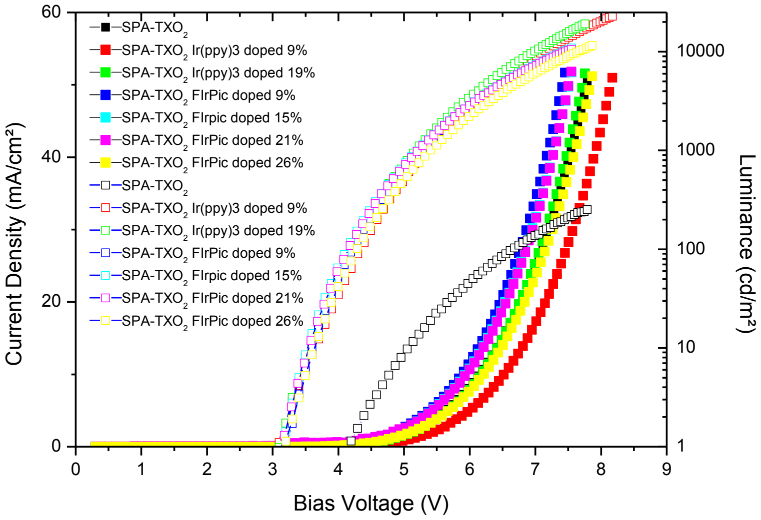

S14. Luminance (hollow) and current density (solid) over voltage for SPA-TXO$_2$ devices

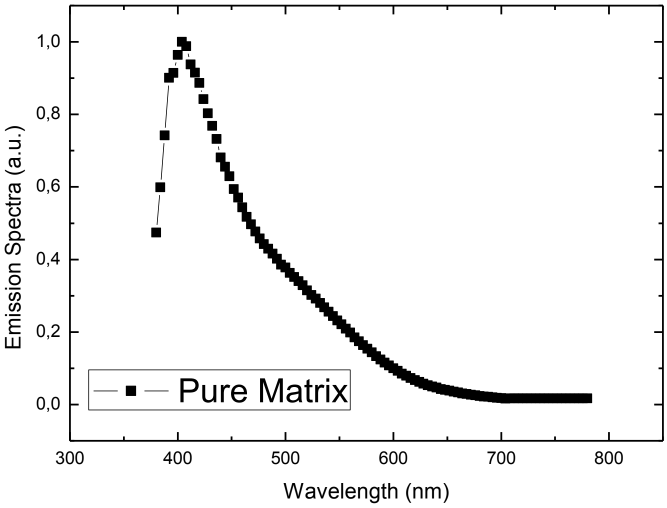

S15. Non-doped EL spectra

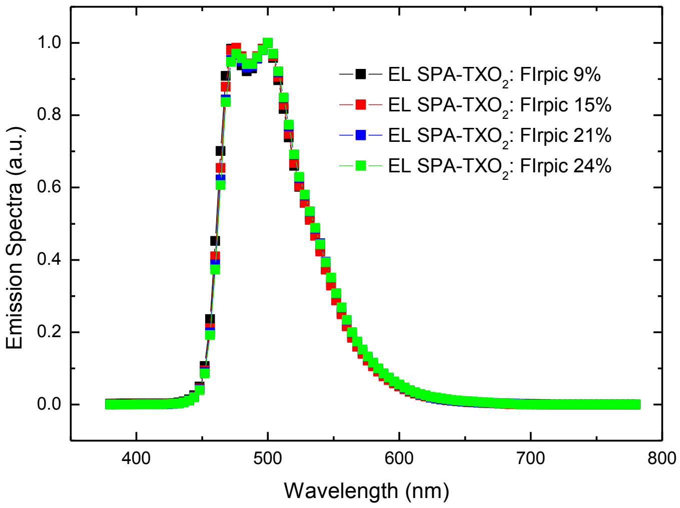

S16. FIrpic doped EL spectra

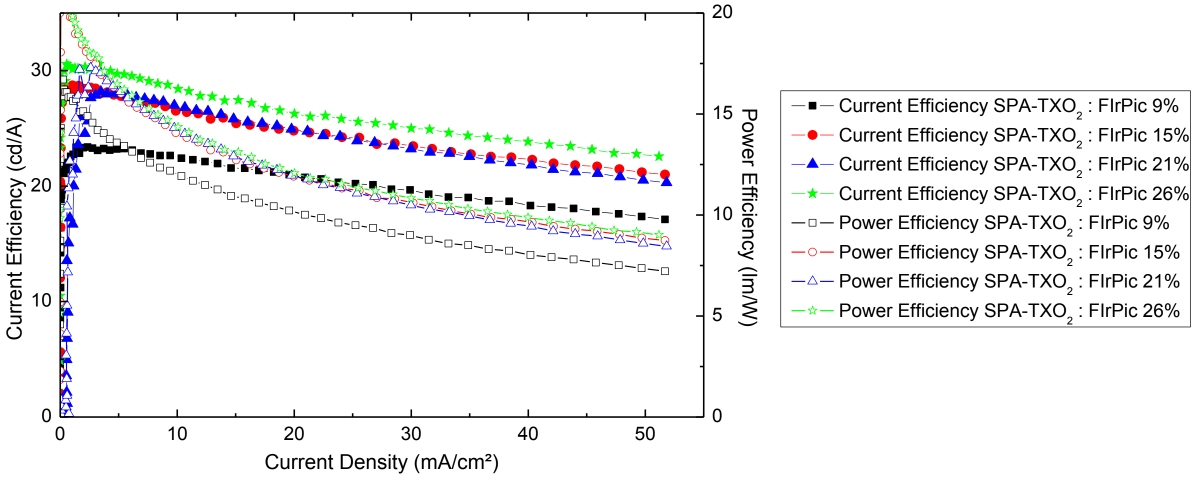

S17. FIrpic devices efficiencies

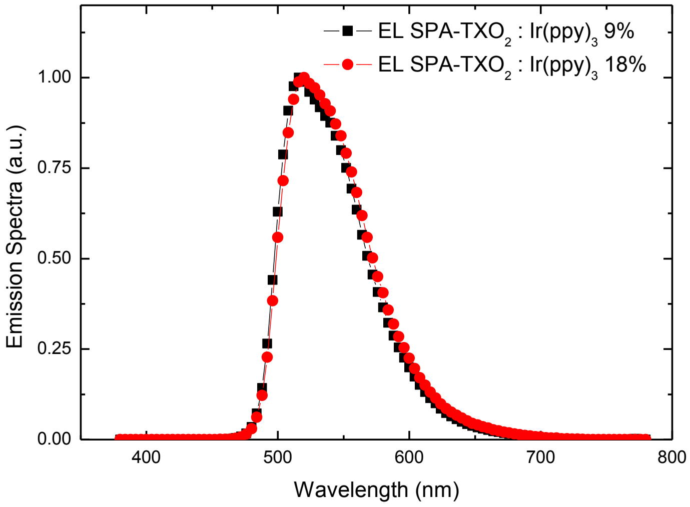

S18. Ir(ppy)$_3$ devices EL spectra

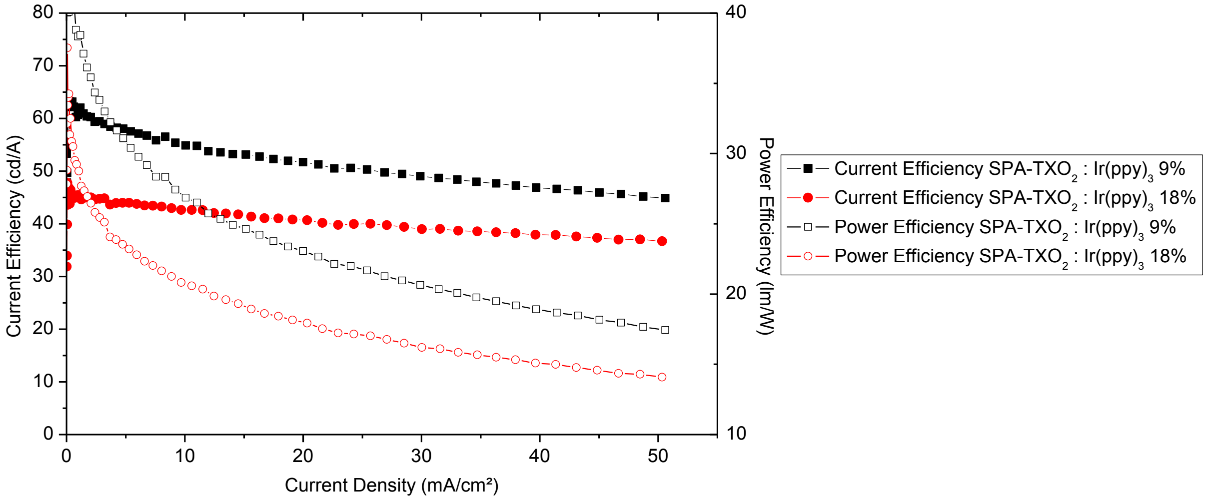

S19. Ir(ppy)$_3$ devices efficiencies

mCP Devices

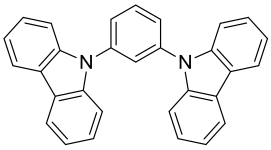

1,3-di(9*H*-carbazol-9-yl)benzene

S20. Structure of mCP

Table 8.Properties of mCP devices

Sample	Vs^{a} [V]	EQE^{b} [%]	Current Efficiency^{b} [cd/A]	Power Efficiency^{b} [lm/W]	CIE (x;y) at 10 mA/cm²
FIrpic 26%	3.2	8.6 / 13.7 / 15.3	12.4 / 19.7 / 22.1	10.3 / 12.6 / 11.6	0.19; 0.46

a\ at 1 cd.m^{-2}, **b**\ at 10 mA.cm^{-2} / at 100 cd.m^{-2} / at 1000 cd.m^{-2}..

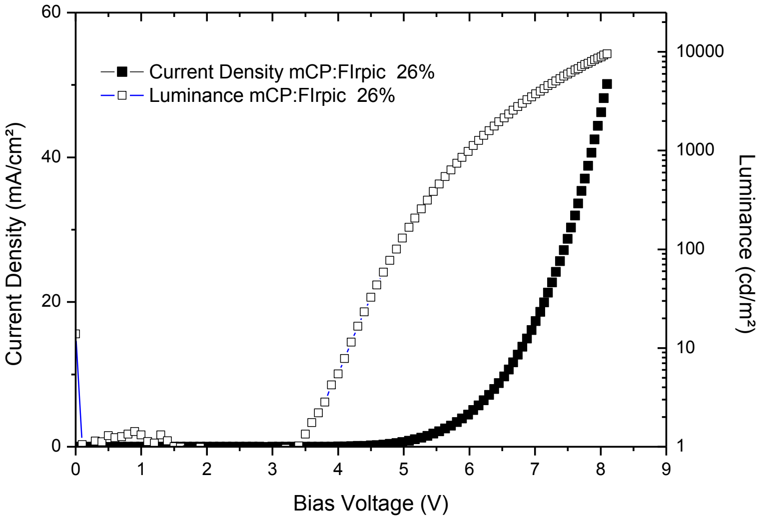

S21. Luminance (hollow) and current density (solid) over voltage

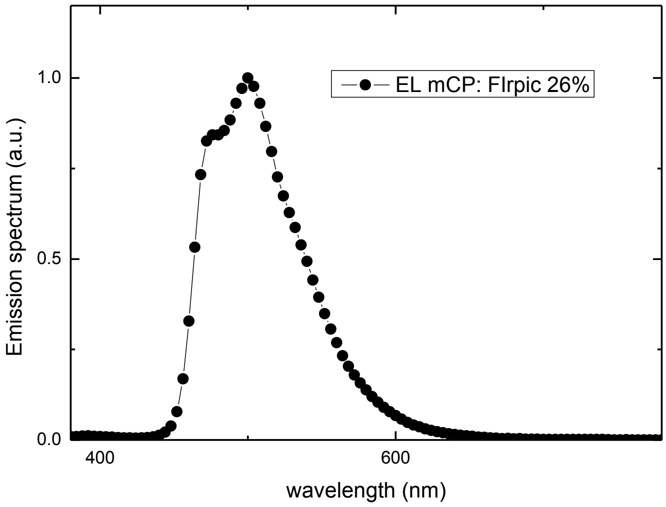

S22. FIrpic doped EL spectra

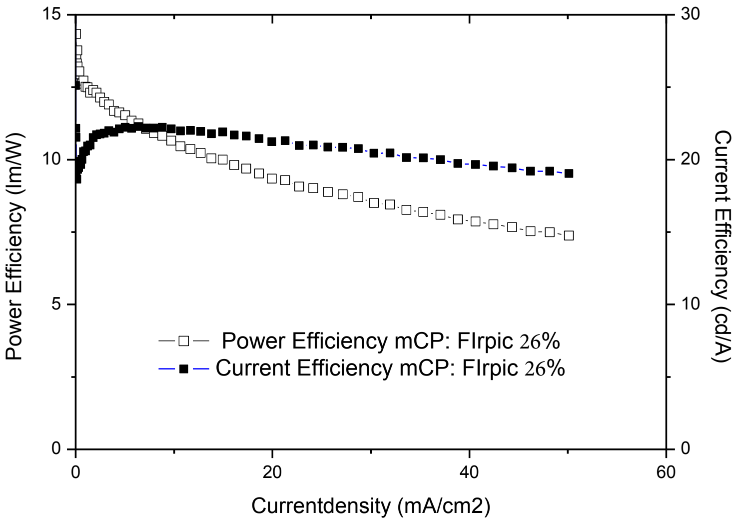

S23. <u>FIrpic devices efficiencies</u>

Copy of analysis spectra

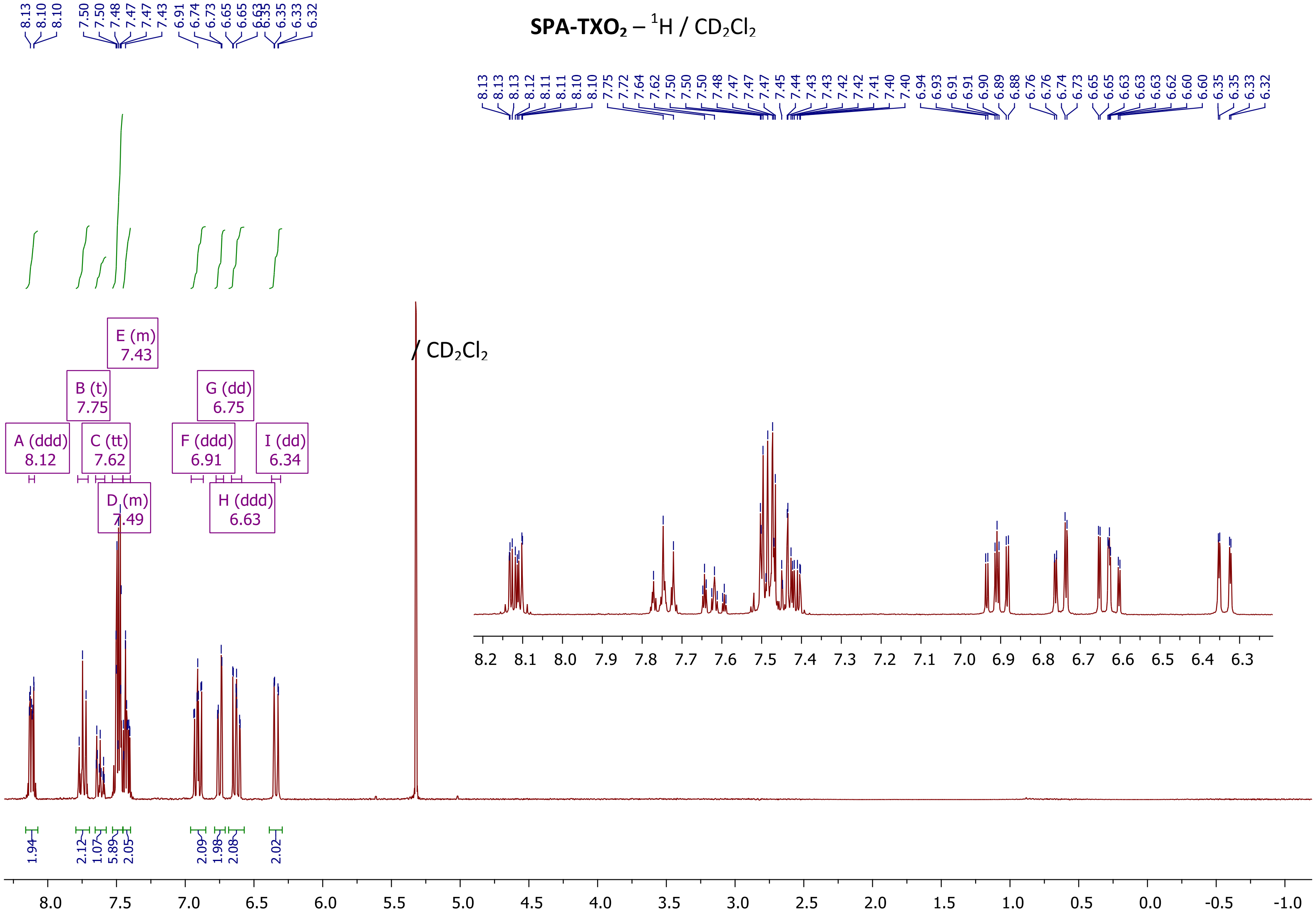

SPA-TXO$_2$ – COSY-90 / CD$_2$Cl$_2$

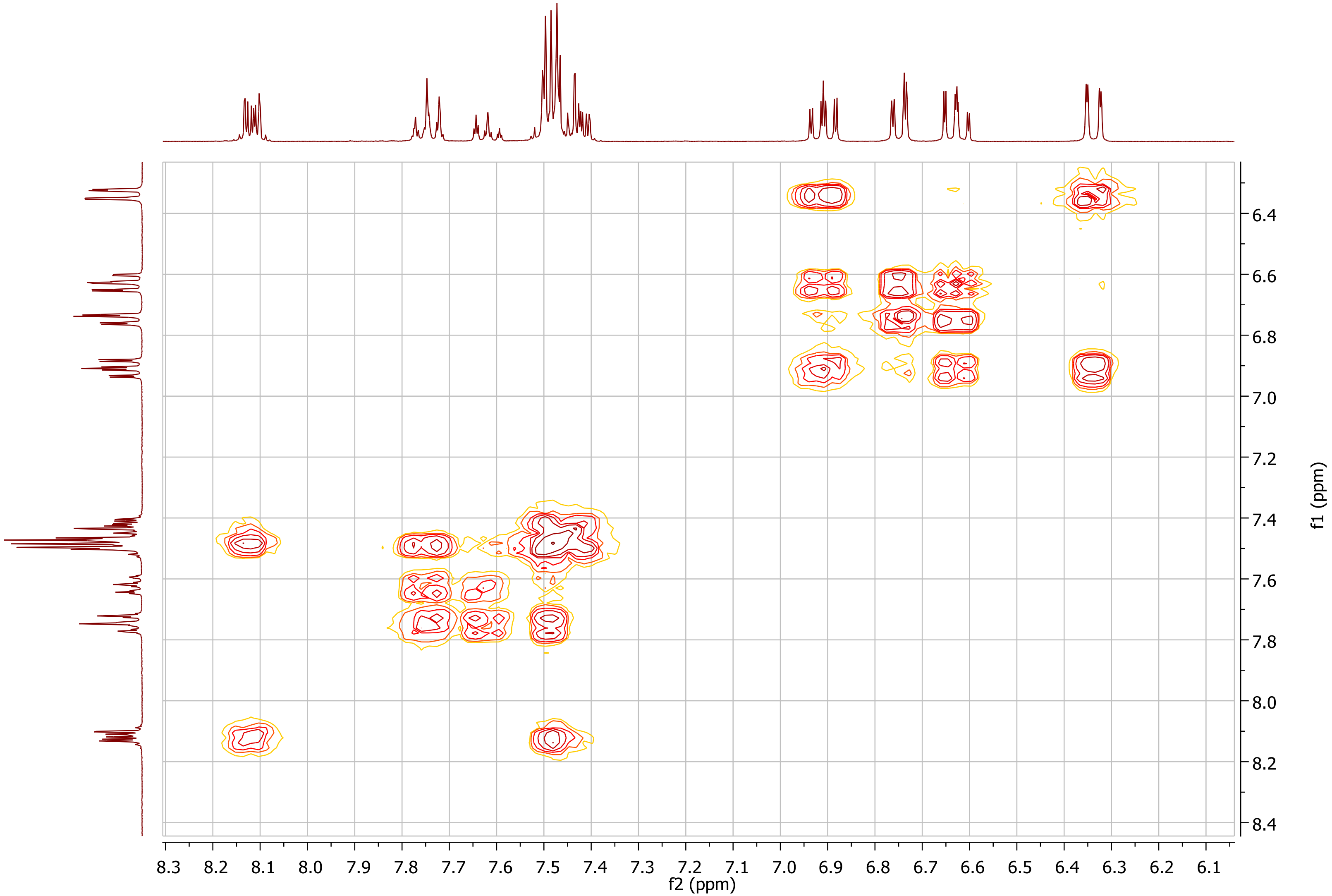

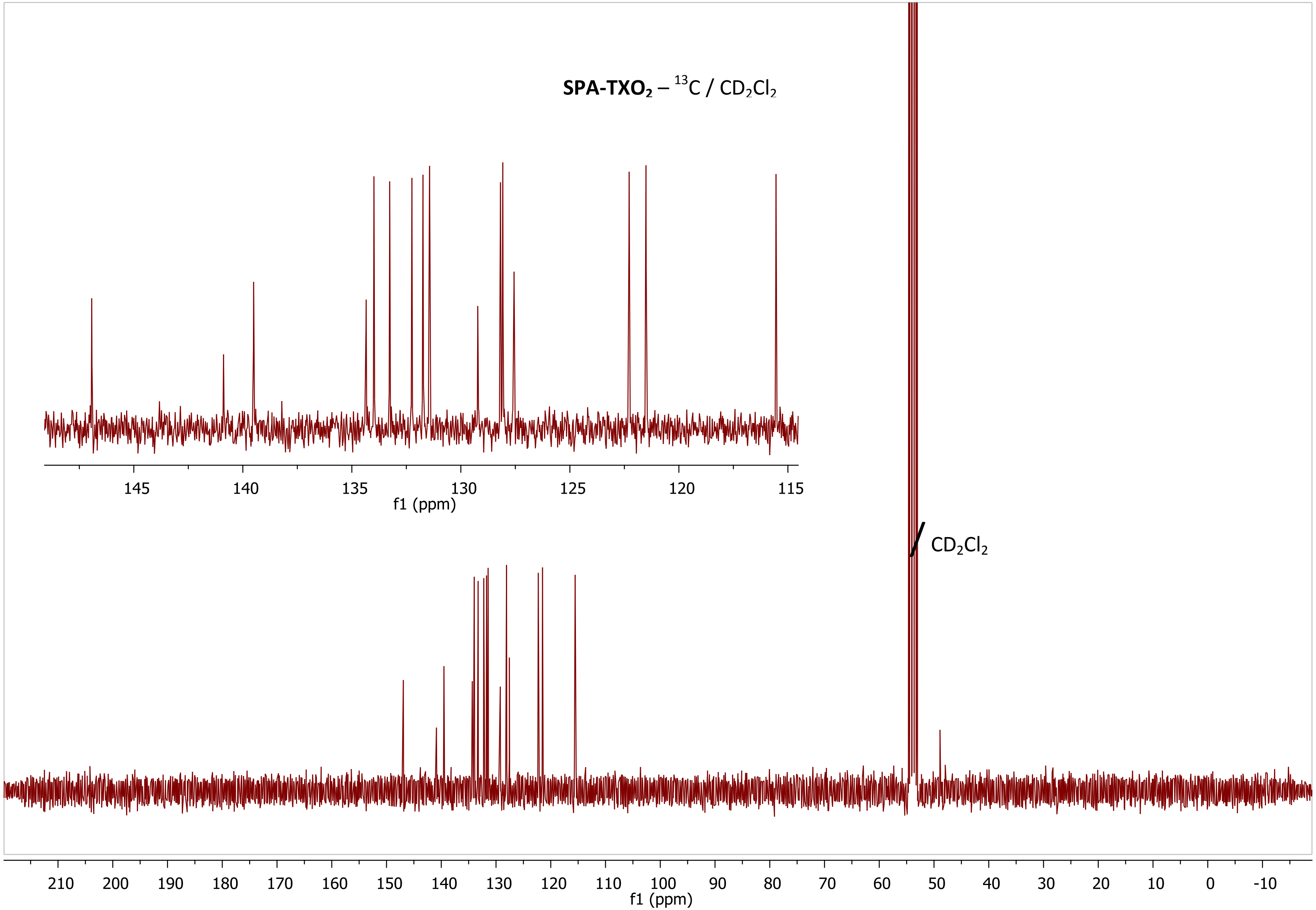
SPA-TXO$_2$ – ^{13}C / CD$_2$Cl$_2$
145
140
135
130
125
120
115
f1 (ppm)
CD$_2$Cl$_2$
210
200
190
180
170
160
150
140
130
120
110
100
90
80
70
60
50
40
30
20
10
0
-10
f1 (ppm)

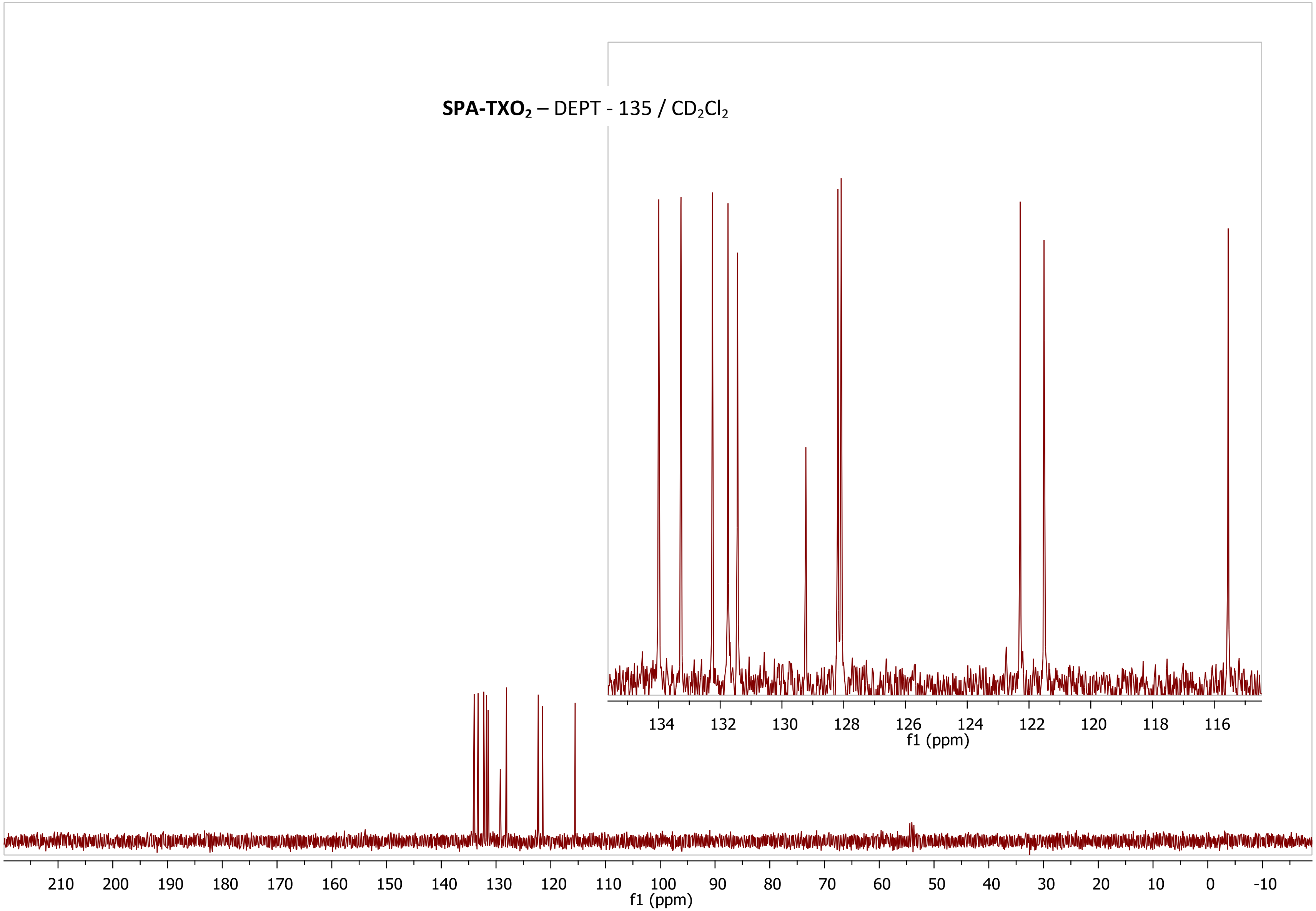

SPA-TXO$_2$ – DEPT - 135 / CD_2Cl_2

SPA-TXO$_2$ – HSQC / CD_2Cl_2

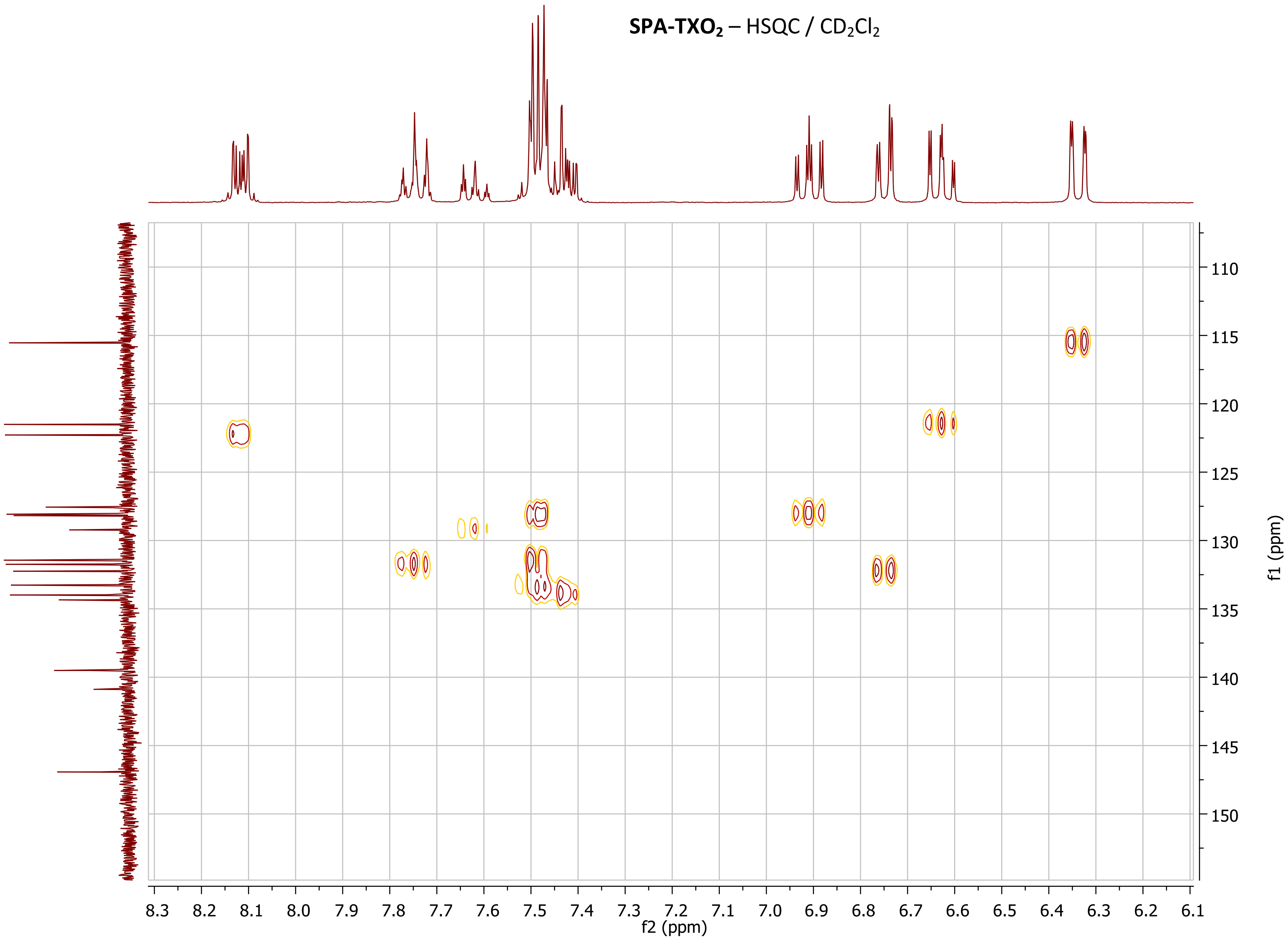

SPA-TXO$_2$ – portion of HSQC
showing the 3 C-H correlations of multiplet Hd

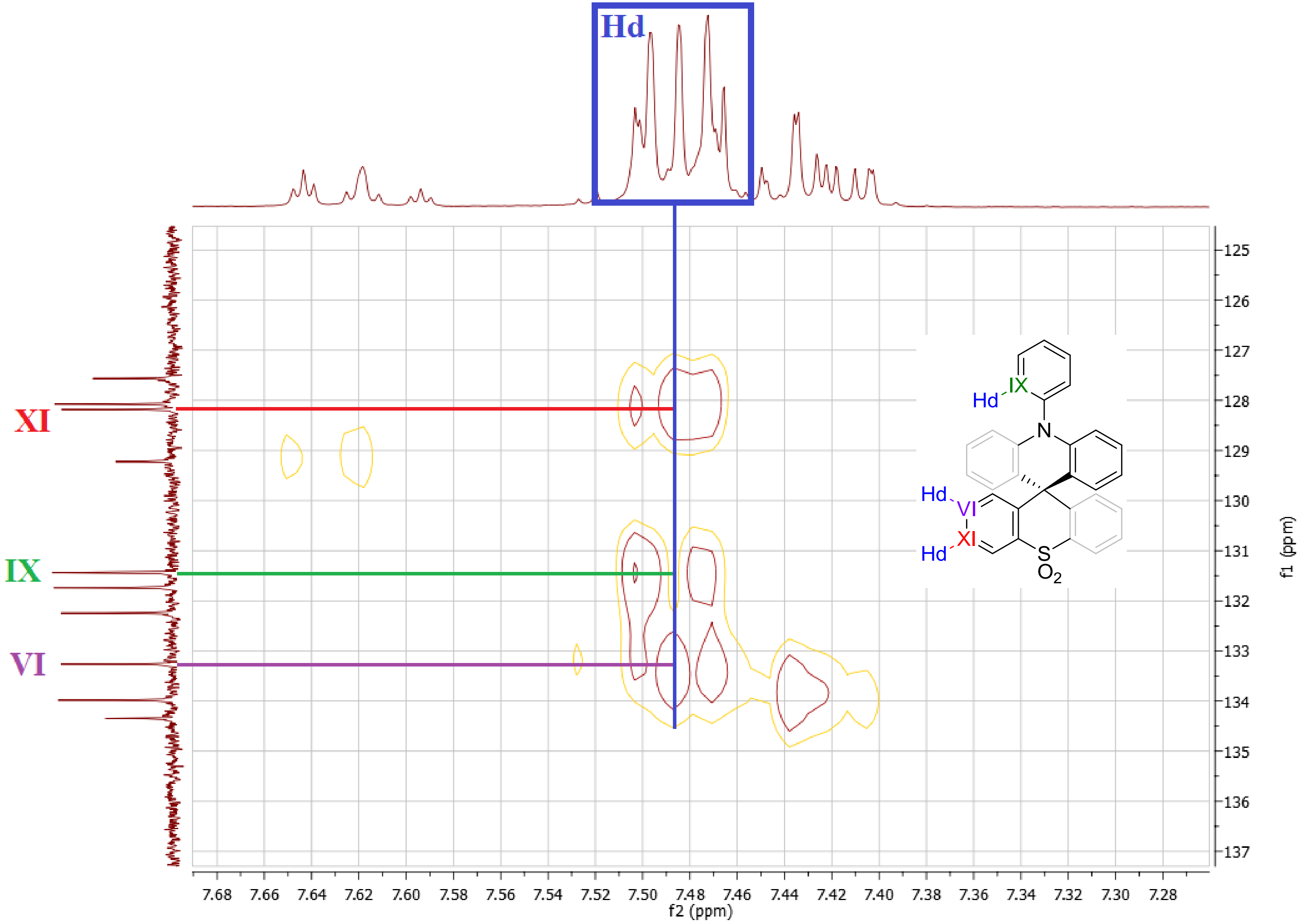

SPA-TXO$_2$ – HMBC / CD$_2$Cl$_2$

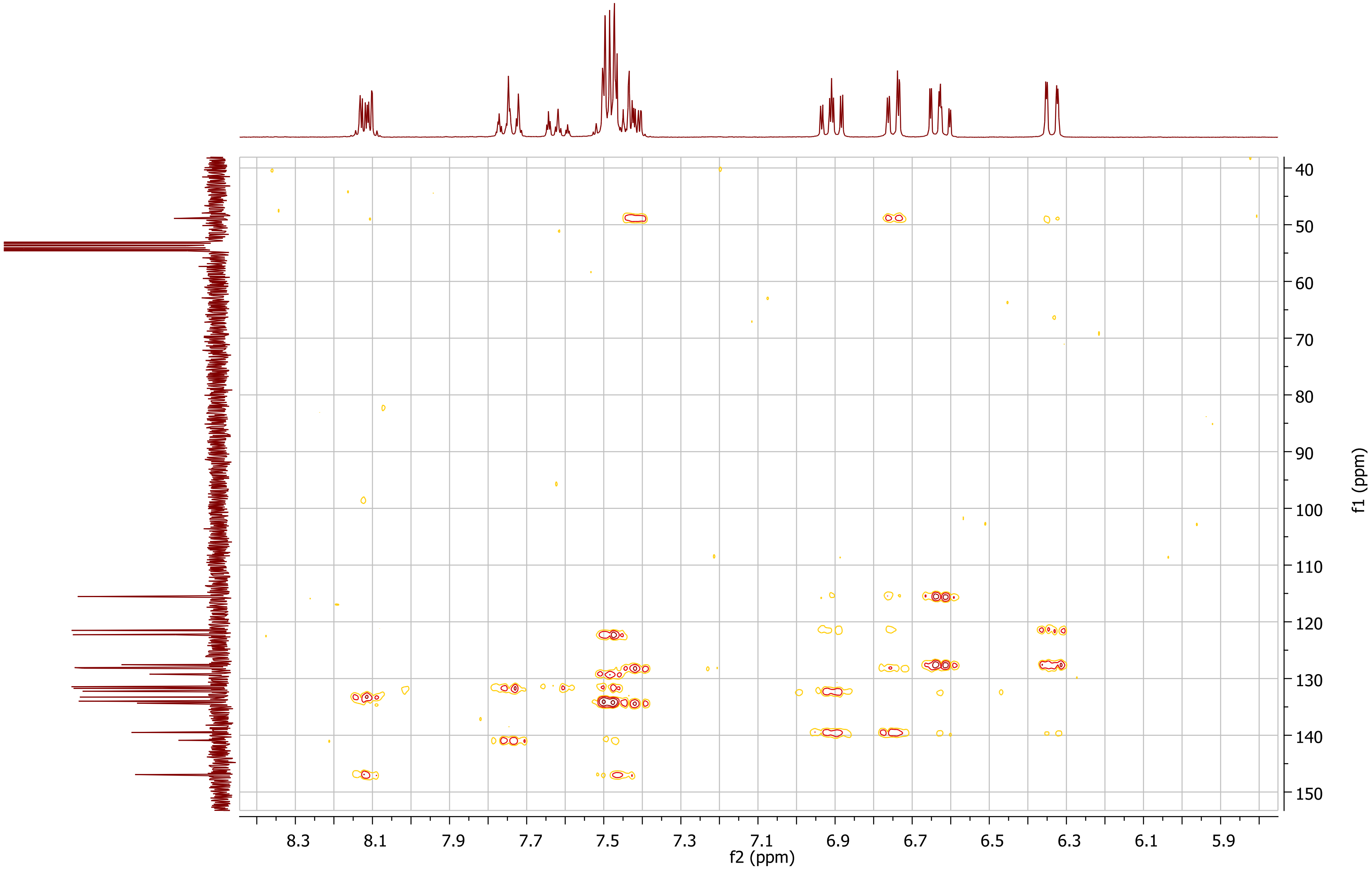

SPA-TXO$_2$ – portion of HMBC
showing C-H correlations with the Spiro Carbon (XVII)

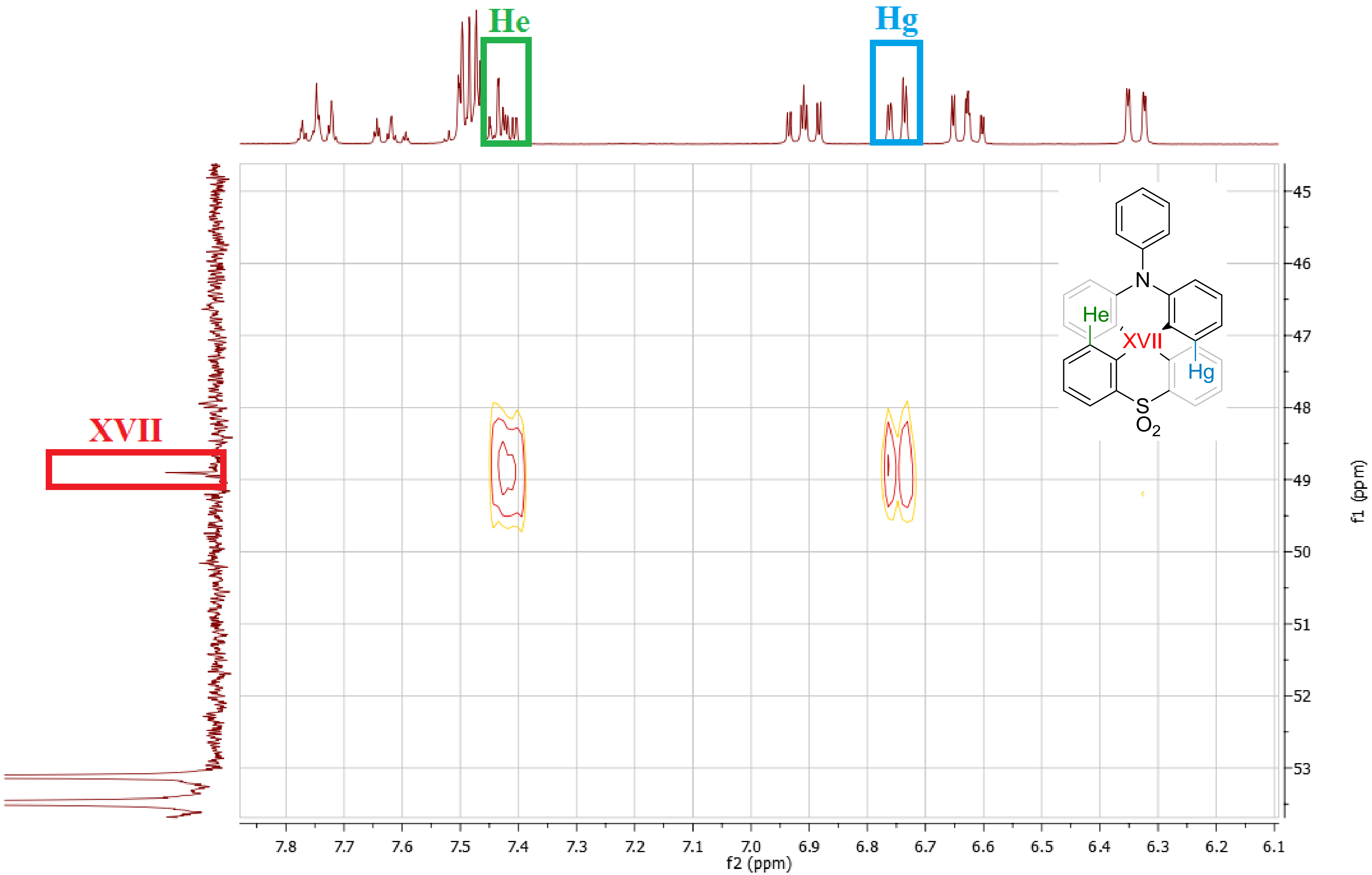

Rapport d'analyse de l'échantillon MR SPA TXO2

Spectre et traitement réalisés au Centre régional de mesures physiques de l'Ouest - Université de Rennes 1

Instrument : Waters Q-Tof 2 Fichier : ASAP_1930_MS_01.raw Date/Heure : 27-Feb-2014 / 12:40:30 Scans : (24 : 57) de m/z 80 à 800 Lockmass : 391
Description : M. ROMAIN MR SPA TXO2 FL Température : 500°C

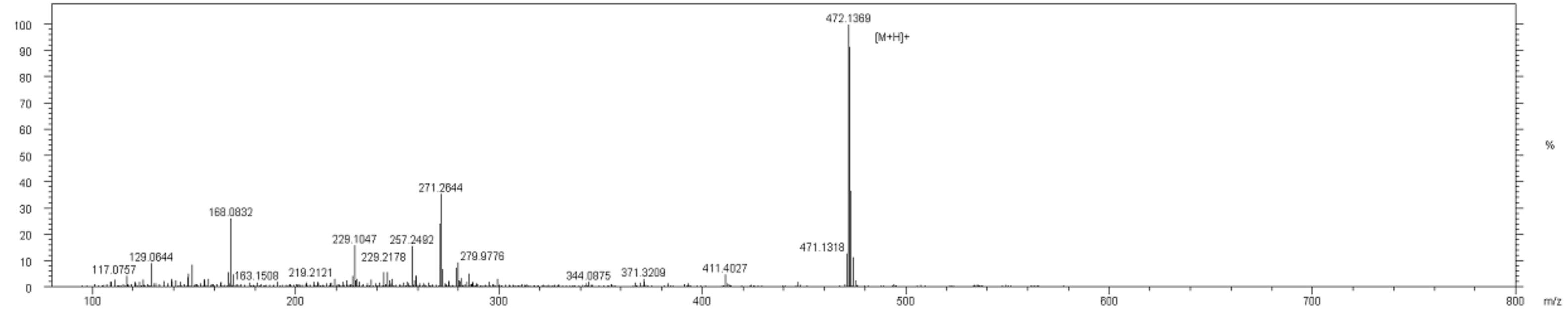

Instrument : Waters Q-Tof 2 Fichier : ASAP_1930_MS_01.raw Date/Heure : 27-Feb-2014 / 12:40:30 Scans : (24 : 57) de m/z 469 à 478 Lockmass : 391
Description : M. ROMAIN MR SPA TXO2 FL Température : 500°C

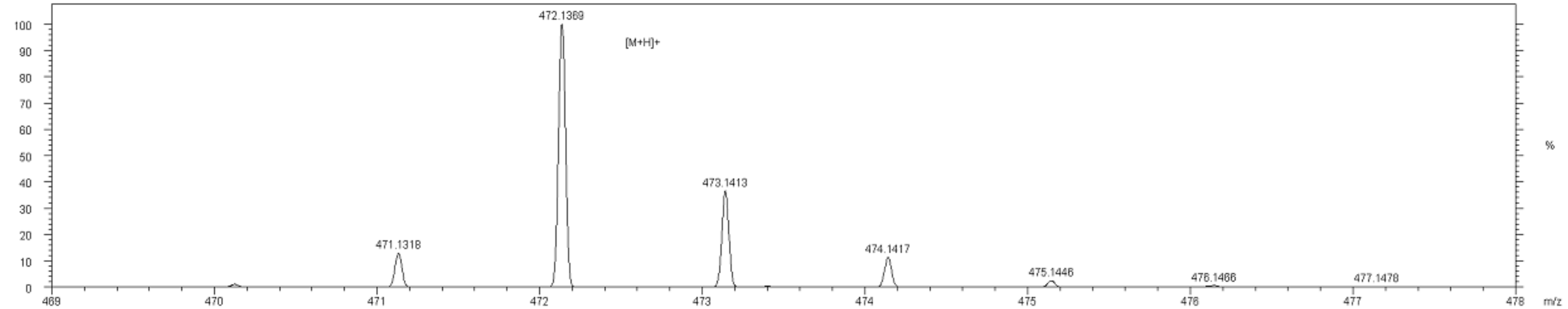

Séparation : 10 Seuil : 0.01 mmu Charge : 1 Résolution : 10000
Formule brute : C31 H22 N O2 S

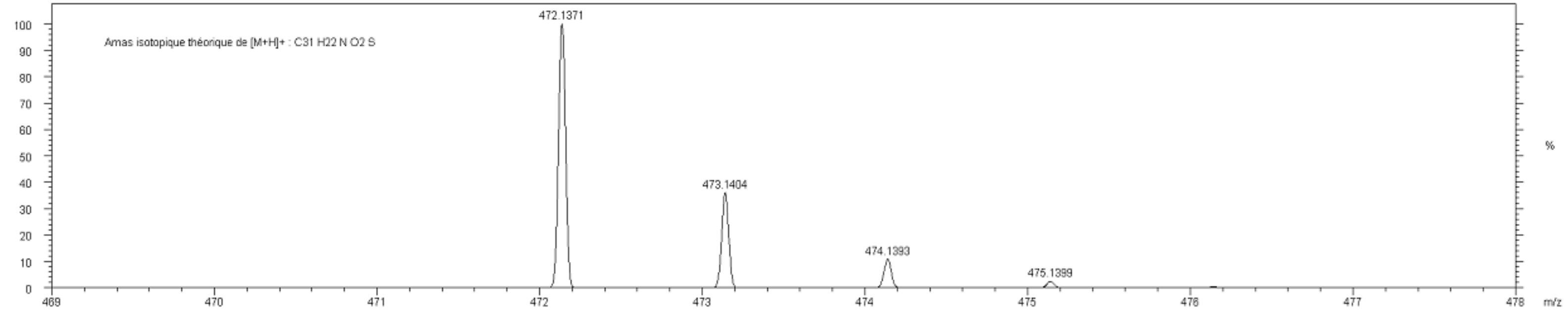

(1) Altomare, A.; Burla, M. C.; Camalli, M.; Cascarano, G. L.; Giacovazzo, C.; Guagliardi, A.; Moliterni, A. G. G.; Polidori, G.; Spagna, R. *J. Appl. Crystallogr.* **1999**, *32*, 115.

(2) Sheldrick, G. M. *Acta Crystallographica Section A* **2008**, *64*, 112.

(3) Farrugia, L. *J. Appl. Crystallogr.* **1999**, *32*, 837.

(4) Kulkarni, A. P.; Tonzola, C. J.; Babel, A.; Jenekhe, S. A. *Chem. Mater.* **2004**, *16*, 4556.

(5) Cardona, C. M.; Li, W.; Kaifer, A. E.; Stockdale, D.; Bazan, G. C. *Adv. Mater. (Weinheim, Ger.)* **2011**, *23*, 2367.

(6) Hohenberg, P.; Kohn, W. *Physical Review* **1964**, *136*, B864.

(7) Calais, J.-L. *Int. J. Quantum Chem.* **1993**, *47*, 101.

(8) Becke, A. D. *Phys. Rev. A* **1988**, *38*, 3098.

(9) Becke, A. D. *The Journal of Chemical Physics* **1993**, *98*, 5648.

(10) Becke, A. D. *The Journal of Chemical Physics* **1993**, *98*, 1372.

(11) Lee, C.; Yang, W.; Parr, R. G. *Physical Review B* **1988**, *37*, 785.

(12) Frisch, M. J.; Trucks , G. W.; Schlegel, H. B.; Scuseria, G. E.; Robb, M. A.; Cheeseman, J. R.; Scalmani, R.; Barone, G.; Mennucci, B.; Petersson, G. A.; Nakatsuji, H.; Caricato, M.; , X. L.; Hratchian, H. P.; Izmaylov, A. F.; Bloino, J.; Zheng, G.; Sonnenberg, J. L.; Hada, M.; Ehara, M.; Toyota; , K.; Fukuda, R.; Hasegawa, J.; Ishida, M.; Nakajima, T.; Honda, Y.; Kitao, O.; Nakai, H.; Vreven, T.; Montgomery, J. A. J.; Peralta, J. E.; Ogliaro, F.; Bearpark, M.; Heyd, J. J.; Brother, E.; Kudin, K. N.; Staroverov, V. N.; Kobayashi, R.; Normand, J.; Raghavachari, K.; Rendell, A.; Burant, J. C.; Iyengar, S. S.; Tomasi, J.; Cossi, M.; Rega, N.; Millam, N. J.; Klene, M.; Knox, J. E.; Pomelli, C.; Ochterski, J. W.; Martin, R. L.; Morokuma, K.; Zakrzewski, V. G.; Voth, G. A.; Salvador, P.; Dannenberg, J. J.; Dapprich , S.; Daniels, A. D.; Farkas, O.; Foresman, J. B.; Ortiz, J. V.; Cioslowski, J.; Fox , D. J. *Gaussian 09, version A02, Gaussian, Inc., Wallingford, CT* **2009.**

(13) Amriou, S.; Wang, C.; Batsanov, A. S.; Bryce, M. R.; Perepichka, D. F.; Ortí, E.; Viruela, R.; Vidal-Gancedo, J.; Rovira, C. *Chemistry – A European Journal* **2006**, *12*, 3389.

(14) Haynes, W. M. *CRC Handbook of Chemistry and Physics*, 2011.